Ann. Geophysicae 12, 1207–1217 (1994) © EGS – Springer-Verlag 1994

Annales Geophysicae

Penetration of solar radiation in the Schumann-Runge bands of molecular oxygen: a robust approximation

G. Kockarts

Institut d'Aéronomie Spatiale, 3 avenue Circulaire, B–1180 Brussels, Belgium

Received: 11 April 1994 / Revised: 21 May 1994 / Accepted: 1 June 1994

Abstract. The Schumann-Runge bands of molecular oxygen between 175 nm and 205 nm cover a spectral region of great importance for the effect of solar radiation in the middle atmosphere. The highly structured absorption cross sections that can be computed with good accuracy lead to prohibitive computer resources, however, when they have to be used in complex atmospheric models. Although various approximations have been developed, another approach is proposed to avoid spurious effects, even when the new approximations are used outside of their validity range, corresponding to a solar attenuation of the order of 10^{-10}. Comparisons between exact computations and present approximations lead to satisfactory agreement.

1 Introduction

The Schumann-Runge band system ($B^3\Sigma_u^- \leftarrow X^3\Sigma_g^-$) of molecular oxygen between 175 nm and 205 nm corresponds to a wavelength region that is of fundamental importance for the penetration of solar radiation in the middle atmosphere below 100 km altitude (see, for instance, Banks and Kockarts, 1973).

The atlas of Yoshino *et al.* (1984) clearly indicates that numerous rotational lines influence the absorption of solar radiation and require, as a consequence, high resolution absorption cross sections. Ackerman and Biaumé (1970) determined vibrational and rotational constants from high-resolution photographic spectra. These data were used (Ackerman *et al.* 1970) to measure the first high-resolution absorption cross sections at some well-defined wavelengths. Using these results, it was possible to make a detailed computation of the penetration of solar radiation in the Schumann-Runge bands with a resolution of 0.5 cm^{-1} (Kockarts, 1971). These computations are time and memory consuming, however, when they are introduced in large and complex photochemical models of the atmosphere. Therefore, a numerical approximation, taking into account the temperature dependence of the cross sections, was developed for practical applications (Kockarts, 1976). Other approximations are mentioned in the radiative processes section of W.M.O. (1986).

In the present paper, Sect. 2 gives a brief description of the absorption cross sections (Minschwaner *et al.*, 1992) used for computing the penetration of solar radiation in the Schumann-Runge bands with a spectral resolution of 0.5 cm^{-1}. Sect. 3 contains calculations of the exact solar absorption and new numerical approximations are developed for 500 cm^{-1} wave number intervals between 49 000 cm^{-1} and 57 000 cm^{-1}. These approximations are given as sums of six always-decreasing exponentials in order to avoid numerical accidents when the slant total content of O_2 becomes very large. Finally, some applications are presented in Sect. 4 as possible examples for the new robust approximation. Section 5 summarizes the main results.

2 O_2 cross sections and temperature dependence

Within the limits of experimental error and resolution, Hudson and Carter (1969) could not detect any significant change in the absorption cross sections of the O_2 Schumann-Runge bands when temperature varies between 200 K and 300 K. However, absorption cross sections measured at some known wavelengths (Ackerman *et al.*, 1970) could be fitted only with a 300-K theoretical spectrum and not with a 200-K spectrum. This implies that temperature-dependent cross sections have to be used for the analysis of solar radiation absorption in the Schumann-Runge bands of O_2 (Kockarts, 1971). The variation with temperature is due essentially to temperature dependence of the population of the first vibrational level of the ground state of the molecule and to the temperature dependence of the relative intensities of the rotational lines in a specific band. For the development of numerical approximations of the solar radiation penetration in the middle atmosphere, Kockarts (1976) used 17 sets of cross sections corresponding to temperatures between 160 K and 320 K, with a 10-K interval. Later, Murtagh

Correspondence to: G. Kockarts

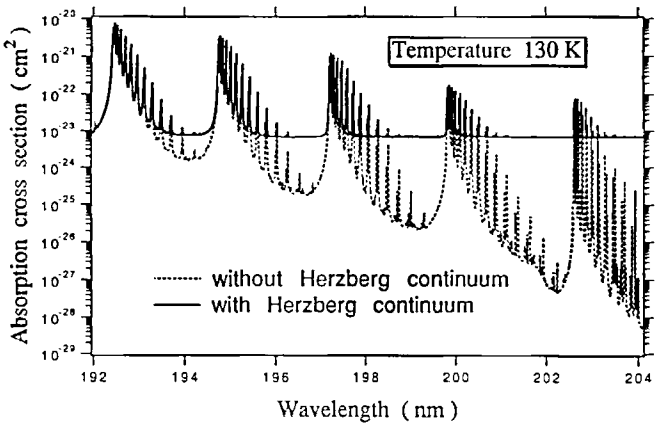

Fig. 1. Absorption cross section in the wavelength region where Herzberg continuum can influence the Schumann-Runge cross section for 130 K temperature

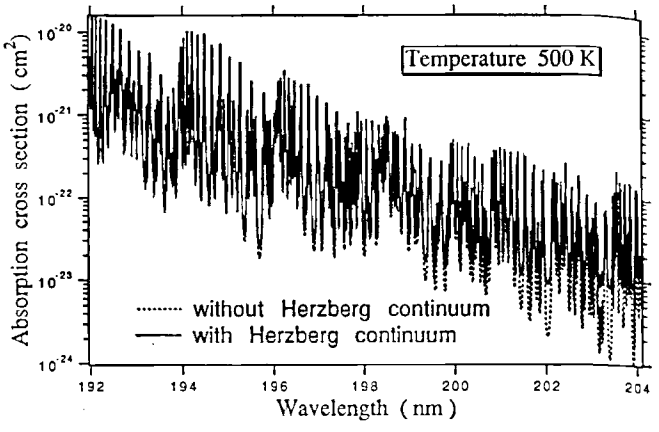

Fig. 2. Absorption cross section in the wavelength region where Herzberg continuum can influence the Schumann-Runge cross section for 500 K temperature

(1988, 1989) used five sets between 150 K and 300 K with a 50-K interval.

High-resolution absorption cross sections have been measured by Yoshino *et al.* (1983, 1987) at temperatures of 300 K and 79 K. These data have been used by Minschwaner *et al.* (1992) to develop a polynomial fitting of the cross sections for any temperature between 130 K and 500 K, with a spectral resolution of 0.5 cm^{-1}. The agreement with experimental data is excellent and the polynomial fitting allows calculations of atmospheric transmissions with the real vertical temperature distributions. Instead of computing in advance a number sets of cross sections using the most recent molecular parameters, the polynomial coefficients of Minschwaner *et al.* (1992) will be used in the present paper to develop the new numerical approximations. This attractive approach has a further advantage since the underlying Herzberg continuum on the long wavelength side of the Schumann-Runge band system has not been included in the polynomial fitting procedure. This continuum can, therefore, be taken into account by a simple addition to the high-resolution (0.5 cm^{-1}) absorption cross sections for wavelengths greater then approximately 190 nm. The Schumann-Runge continuum on the short wavelength side of the band system is, however, taken into account by Minschwaner *et al.* (1992), using the results of Lewis *et al.* (1985a, b).

Figure 1 shows the absorption cross section on the long wavelength side of the Schumann-Runge bands for a temperature of 130 K. The computations have been made with the polynomial coefficients of Minschwaner *et al.* (1992). Two cases are presented: one without the contribution of the Herzberg continuum and one taking into account this contribution with the cross sections of Yoshino *et al.* (1988). It appears that the Herzberg continuum plays a role down to 193 nm for a temperature of 130 K. The numerical fit given by Eq. (3) of Yoshino *et al.* (1988) is valid from 194 nm to 240 nm. In order to avoid a discontinuity in the cross sections of Fig. 1 at 194 nm, the same equation has been used between 194 nm and 190 nm. Figure 1 shows that, even for a very low temperature, the contribution of the

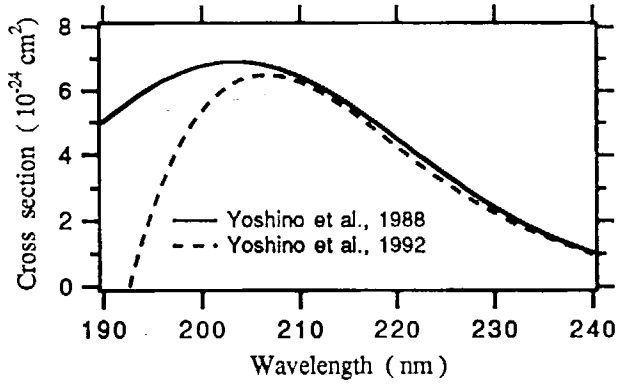

Fig. 3. Two approximations of the Herzberg continuum cross sections between 190 nm and 240 nm

Herzberg continuum to the total cross section is negligible below 193 nm.

Figure 2 has been computed in the same way, but for a temperature of 500 K. The effect of vibrational excitation of the ground level of the Schumann-Runge system is responsible for the increase in complexity of the cross sections. Furthermore, the temperature dependence of the bands' cross sections is such that the influence of the Herzberg continuum is not so important. There is no significant difference between the two curves in Fig. 2 for wavelengths shorter than 200 nm.

The most recent data of Yoshino *et al.* (1992) are shown in Fig. 3 with the data (Yoshino *et al.*, 1988) used in the present paper. The polynomial approximation of the 1992 data should not be used for wavelengths shorter than 193 nm, since it then leads to negative cross sections. The same restriction does not apply to the 1988 data, since they were fitted to another analytical expression. The difference between the two data sets becomes important below 200 nm and would certainly influence the total cross sections in Fig. 1 at low temperature between 193 nm and 200 nm. Minschwaner *et al.* (1993) have used both sets of cross sections to compute O_2 transmittances observed in the stratosphere by Anderson and Hall (1986). They found that the agreement with the

balloon observations was significantly poorer when using the lower values of Yoshino *et al.* (1992). Apparently, a problem still exists between 193 nm and 200 nm for the Herzberg continuum. A sensitivity analysis of stratospheric composition in a two-dimensional model has recently been made by Toumi and Bekki (1994). It indicates that significant differences can result for minor constituents in the lower stratosphere.

Although the higher values of Yoshino *et al.* (1988) are used in the next section, an approximation of the penetration of solar radiation will also be developed without any inclusion of the Herzberg continuum. This will allow the potential user to make his own choice for the absorption in the Herzberg continuum. It is not clear whether or not a temperature dependence of the Herzberg continuum should be included, although experimental data of Johnston *et al.* (1984) do not indicate a significant temperature effect above 205 nm.

3 Reduction factors and their approximations

For a monochromatic radiation, the absorption of solar photons is governed by Beer-Lambert's law. The Schumann-Runge bands system can be assimilated to a set of 16000 spectral points with different cross sections at every 0.5 cm^{-1} between 49000 and 57000 cm^{-1}. The whole spectral interval is divided into 16 subintervals, each having a width of 500 cm^{-1}. Using the formulation given by Kockarts (1971, 1976), it is possible to define reduction factors for each 500 cm^{-1} interval as

$$R_j(\mathrm{M}) = \frac{1}{1000}\sum_{i=1}^{1000} \exp(-\tau_{ij}), \tag{1}$$

and

$$R_j(\mathrm{O_2}) = \frac{1}{1000}\sum_{i=1}^{1000} \epsilon_j \sigma_{ij} \exp(-\tau_{ij}), \tag{2}$$

where j corresponds to a 500 cm^{-1} interval, τ_{ij} is the slant optical depth for O_2 in interval j for wave number corresponding to index i, ϵ_j is the predissociation efficiency in interval j, and σ_{ij} is the O_2 absorption cross section.

The dimensionless reduction factors $R_j(\mathrm{M})$ are equivalent to the transmission functions used by Fang *et al.* (1974) and the $R_j(O_2)$ in cm^2 are equivalent to the expressions used by them for the computation of the O_2 photodissociation coefficient. However, these authors do not put the absorption cross section under the integral sign for computing the optical depth

$$\tau_{ij} = \int_s^\infty \sigma_{ij} n(\mathrm{O_2})\, ds, \tag{3}$$

where $n(O_2)$ is the molecular oxygen concentration and s is the slant path.

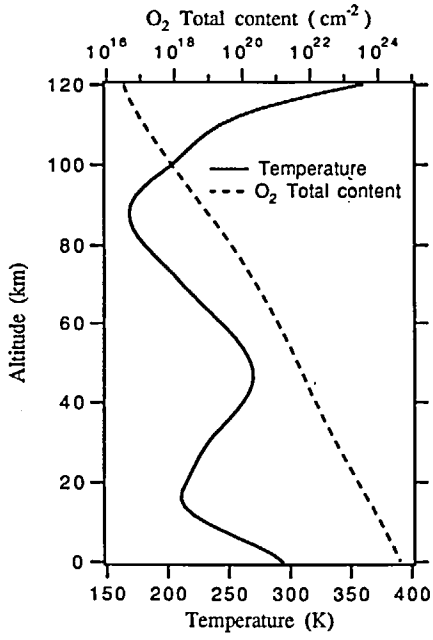

Fig. 4. Atmospheric model (Hedin, 1991) for geophysical conditions indicated in the text

As a consequence, their opacity distribution functions method does not fully account for the temperature dependence effect.

In the present work, the reduction factors are computed in every 500 cm^{-1} wave number interval with the absorption cross sections of Minschwaner *et al.* (1992). Previous computations of reduction factors are usually made with the U.S. Standard Atmosphere (1976). In the present paper the atmospheric model is taken from Hedin (1991). This analytical semi-empirical model can be applied for any geophysical condition. As input parameters, we have adopted a day number of 180, a latitude of 40°, a longitude 0°, a local solar time of 12 h, solar decimetric flux of 150 Jansky, and a daily planetary geomagnetic index of 4. The choice of the last two values has no significant effect for altitudes below 100 km.

Figure 4 gives the vertical temperature distribution and the O_2 overhead total content used in subsequent computations.

Having computed the reduction factors (1) and (2), the solar irradiance $\phi_j(z)$ at altitude z is given for each 500 cm^{-1} interval by

$$\phi_j(z) = \phi_j(\infty) \times R_j(\mathrm{M}) \times \exp[-\tau_j(\mathrm{O_3})], \tag{4}$$

where $\phi_j(\infty)$ is the solar irradiance at the top of the atmosphere in the wave number interval j and $\tau_j(O_3)$ is the slant optical depth resulting from ozone absorption in the same interval.

The photodissociation coefficient $J_j(\mathrm{M})$ for any minor constituent M at altitude z can be computed by

$$J_j(\mathrm{M}) = \phi_j(z) \times \sigma_j(\mathrm{M}), \tag{5}$$

where $\sigma_j(\mathrm{M})$ is the photodissociation cross section for M in the wave number interval j.

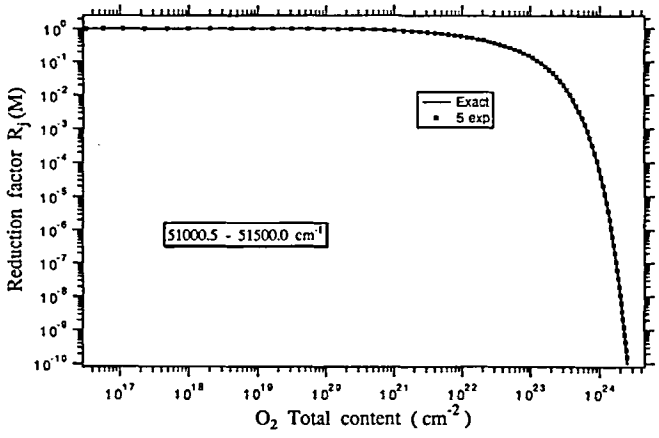

Fig. 5. Comparison between exact calculation and approximation of the reduction factor R_j(M) in the 51 000.5–51 500.0 cm^{-1} interval

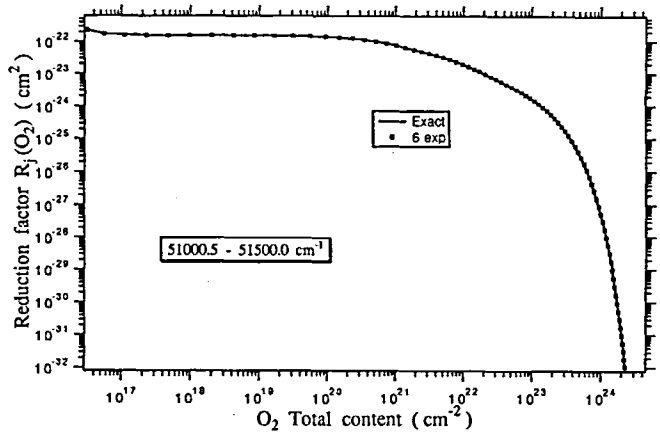

Fig. 6. Comparison between exact calculation and approximation of the reduction factor $R_j(O_2)$ in the 51 000.5–51 500.0 cm^{-1} interval

The photodissociation coefficient $J_j(O_2)$ for molecular oxygen is obtained from expression

$$J_j(O_2) = \phi_j(\infty) \times R_j(O_2) \times \exp -[\tau_j(O_3)]. \quad (6)$$

Rayleigh scattering is neglected in Eqs. (4)–(6).

3.1 Approximations with Herzberg continuum

Almost all previous analytical approximations for the reduction factors (Kockarts, 1976; Blake, 1979; Allen and Frederick 1982; Nicolet and Peetermans, 1980; Murtagh, 1988, 1989; Nicolet and Kennes, 1989) are based on the determination of polynomial coefficients by *linear* least square fitting procedures.

Although this technique is fully appropriate, it presents some danger when the approximations are used for slant O_2 total contents or for optical depths outside of the validity domain usually given by these authors. Furthermore, the validity domain is not identical for each wave number interval, and careful tests are required in the coding. In some cases, misuses can even create photons, i.e. an increase of photodissociation coefficients when the O_2 total content increases!

The definition of the reduction factors given by Eqs. (1) and (2) show that these quantities are a sum of 1000 exponentials with always negative arguments. The present approximation is based on the same mathematical structure. Therefore, the exact expressions are replaced by

$$R_j(M) = a_1 \times \exp(-a_2 \times N) + a_3 \times \exp(-a_4 \times N) + \cdots + a_{11} \times \exp(-a_{12} \times N), \quad (7)$$

and

$$R_j(O_2) = b_1 \times \exp(-b_2 \times N) + b_3 \times \exp(-b_4 \times N) + \cdots + b_{11} \times \exp(-b_{12} \times N), \quad (8)$$

where N is the slant O_2 total content and a_1–a_{12} and b_1–b_{12} are numerical coefficients to be found.

The determination of these coefficients can only be made by *non linear* least square fitting. An excellent technique for such work has been developed by Marquardt (1963), the implementation of which is described by Press *et al.* (1989). However, this technique cannot be applied automatically to the whole set of reduction factors for essentially two reasons. Firstly, initial guesses must be provided for all coefficients. Secondly, the mathematical approach searches for a minimum corresponding to a negligible decrease in statistical chi-square tests. This implies that the first minimum found is not necessarily the deepest one and that another set of initial guesses could lead to better results. In order to weaken this constraint, all reduction factors have been fitted successively with two, three, four, five, and six exponentials. As a consequence, only two coefficients have to be guessed in each partial fit, since the other initial guesses come from the previous fit. Furthermore, a negative value for any coefficient a_i or b_i is rejected. This assures that all terms in Eqs. (7) and (8) strictly decrease as the O_2 total content increases. The problem of creating photons is, therefore, definitely avoided and the approximations can be considered as *robust* with no undesirable effects.

The approximations have been developed to cover a decrease by a factor of 10^{10} for all R_j(M) and $R_j(O_2)$. As an example, Figs. 5 and 6 show the results obtained in the interval 51 000.5–51 500.0 cm^{-1}. One sees that the approximation holds for the 10^{10} range of variation for the reduction factors.

Similar results are obtained for the 16 wave number intervals and the a_i and b_i coefficients are given in Tables 1 and 2, respectively. As usual in tables, a notation such as 1.13E-01 should be understood as 1.13×10^{-01}. The values a_1–a_{12} should be read from left to right on three consecutive lines under each wave number interval. When the coefficients are zero, they are indicated by a dash.

It can be seen that all coefficients are positive and that in some cases a good fit is obtained with less then 6 terms in Eqs. (7) and (8). An example is given in Fig. 5, where the dotted reduction factor represents the fit with five exponential terms.

The temperature effect is apparent in Fig. 6, where the reduction factor $R_j(O_2)$ shows a change in curvature for low total contents. This is a consequence of the higher temperature at 120 km altitude. When Minschwaner *et al.*

(1993) and Minschwaner and Siskind (1993) used the opacity distribution functions (ODF), they noted that the choice of an appropriate temperature is important. In each spectral interval, they chose the temperature corresponding to the altitude at which optical depth is unity. This indicates that the ODF method is not fully temperature dependent. Although Eqs. (7) and (8) have a similar form to the ODF approximation of Minschwaner *et al.* (1993) and Minschwaner and Siskind (1993), they take into account the temperature at each level for the computation of the absorption cross sections.

The accuracy of the approximations is estimated by computing exactly the total reduction factors $R(\mathrm{M})$ and $R(\mathrm{O_2})$ over the interval from 49 000.5 to 57 000.0 $\mathrm{cm^{-1}}$, i.e. 16 000 points for each total factor. The error of the approximation is then evaluated in percent, as

$$\text{Error} = 100 \times [(1/16)\sum_{j=1}^{16} R_j(\mathrm{M}) - R(\mathrm{M})] / R(\mathrm{M}), \tag{9}$$

where the $R_j(\mathrm{M})$ are computed with Eq. (7) and the coefficients in Table 1.

A similar error is defined for $R(\mathrm{O_2})$ and the results are shown in Figs. 7 and 8, respectively. It is seen that the error never exceeds a few percent for all values of the total reductions $R(\mathrm{M})$ and $R(\mathrm{O_2})$ in a domain extending over a factor of 10^{10} variation. Such a test corresponds to the hypothetical case of a constant unitary solar irradiance over the whole interval which is subdivided into 16 parts.

I have also computed a_i and b_i coefficients, as given in Tables 1 and 2 for 1 nm wavelength intervals. The accuracy is less then for 500 $\mathrm{cm^{-1}}$ wave number intervals. Errors like those shown on Figs. 7 and 8 can reach ±10%. Therefore, these 1 nm interval coefficients are not given here.

3.2 Approximations without Herzberg continuum

In order to provide a tool for analyzing the effect of various values for the Herzberg continuum cross sections below 205 nm, it is possible to approximate exact calculations without including this continuum.

The total cross section σ_{ij} used in Eqs. (1)–(3) can be written as

$$\sigma_{ij} = \sigma_{ijSR} + \sigma_{jH}, \tag{10}$$

where σ_{ijSR} is the contribution of the Schumann-Runge bands and of the Schumann-Runge continuum taken from Minschwaner *et al.* (1992), and σ_{jH} is the cross section of the Herzberg continuum considered as constant over the 500 $\mathrm{cm^{-1}}$ j interval. The assumption of a constant σ_{jH} over each interval is valid, since it represents a continuum.

Exact reduction factors $R_{jNH}(\mathrm{M})$ and $R_{jNH}(\mathrm{O_2})$, excluding Herzberg continuum, are then computed with Eqs. (1)–(3), using only values for the σ_{ijSR}.

It is easily shown that the complete reduction factors $R_j(\mathrm{M})$ and $R_j(\mathrm{O_2})$ are related to the $R_{jNH}(\mathrm{M})$ and $R_{jNH}(\mathrm{O_2})$ by

$$R_j(\mathrm{M}) = R_{jNH}(\mathrm{M}) \times T_j(\mathrm{H}), \tag{11}$$

and

$$R_j(\mathrm{O_2}) = [R_{jNH}(\mathrm{O_2}) + \sigma_{jH} \times R_{jNH}(\mathrm{M})] \times T_j(\mathrm{H}), \tag{12}$$

where σ_{jH} is the average Herzberg continuum cross section in interval j.

The transmission function $T_j(\mathrm{H})$ due to the Herzberg continuum in interval j is given by

$$T_j(\mathrm{H}) = \exp[-\int_s^\infty \sigma_{jH} n(\mathrm{O_2})\, ds], \tag{13}$$

where all symbols have been previously defined.

Equation (12) indicates that the computation of the $\mathrm{O_2}$ photodissociation coefficient with approximations neglecting the contribution from the Herzberg continuum requires calculation of the second term $\sigma_{jH} \times R_{jNH}(\mathrm{H})$. Omission of this term would lead to unacceptably large errors.

Figures 1 and 2 show that for all atmospheric temperatures, the contribution of the Herzberg continuum can be neglected for wavelengths shorter than 192 nm. For this reason, approximations without Herzberg continuum have been developed only for wave numbers shorter than 52 000 $\mathrm{cm^{-1}}$. The computational technique has been described in Sect. 3.1. The numerical coefficients for $R_{jNH}(\mathrm{M})$ and $R_{jNH}(\mathrm{O_2})$ are given in Tables 3 and 4, respectively. In order to use approximations without Herzberg continuum over the whole interval, it is necessary to replace the last six intervals in Tables 1 and 2 by those of Tables 3 and 4, respectively. Nicolet and Kennes (1989) have used a similar approach, but it is not clear why their polynomial coefficients for wave numbers greater then 52 000 $\mathrm{cm^{-1}}$ are not identical in both cases, the Herzberg continuum being completely negligible above that wave number.

Inspection of Table 4 shows that a few preexponential coefficients are negative. The approximation remains, however, *robust*, since all the coefficients for the exponential arguments are positive. The necessity to slightly relax the condition that all coefficients should be positive as in Sect. 3.1, is easily understood by looking at Figs. 9 and 10, which show the approximations for the worst case between 50 000.5 and 50 500.0 $\mathrm{cm^{-1}}$. Figure 9 indicates that the transmission due to the spectroscopic lines in this interval is high for any $\mathrm{O_2}$ total content. Figure 10 shows the two terms necessary in Eq. (12) for computing the real reduction factor for $\mathrm{O_2}$. There is a wide range of total contents where both terms are comparable. The temperature effect is pronounced for the exact computation of $R_{jNH}(\mathrm{O_2})$ and the local minimum can only be fitted by allowing a negative coefficient for one preexponential factor (see Table 4). For a total content greater than 2×10^{23} $\mathrm{cm^{-2}}$, the approximation of $R_{jNH}(\mathrm{O_2})$ is not good, although it remains *robust*. This is of no practical importance, since for such total contents the term $\sigma_{jH} R_{jNH}(\mathrm{M})$ is largely dominant and at 200 nm the cross section σ_{jH} is not negligible, compared with the band lines cross sections. The interested reader can obtain the coefficients of Tables 1–4 by sending me a DOS-formatted disket.

Table 1. Coefficients for the approximation of R_j(M)

	a_i 56500.5 – 57000.0		cm^{-1}
1.13402E-01	1.00088E-20	3.48747E-01	2.76282E-20
3.47322E-01	1.01267E-19	1.67351E-01	5.63588E-19
2.31433E-02	1.68267E-18	–	–
	a_i 56000.5 – 56500.0		cm^{-1}
2.55268E-03	1.64489E-21	1.85483E-01	2.03591E-21
2.60603E-01	4.62276E-21	2.50337E-01	1.45106E-20
1.92340E-01	7.57381E-20	1.06363E-01	7.89634E-19
	a_i 55500.5 – 56000.0		cm^{-1}
4.21594E-03	8.46639E-22	8.91886E-02	1.12935E-21
2.21334E-01	1.67868E-21	2.84446E-01	3.94782E-21
2.33442E-01	1.91554E-20	1.63433E-01	2.25346E-19
	a_i 55000.5 – 55500.0		cm^{-1}
3.93529E-03	6.79660E-22	4.46906E-02	9.00358E-22
1.33060E-01	1.55952E-21	3.25506E-01	3.43763E-21
2.79405E-01	1.62086E-20	2.10316E-01	1.53883E-19
	a_i 54500.5 – 55000.0		cm^{-1}
2.60939E-03	2.33791E-22	2.08101E-02	3.21734E-22
1.67186E-01	5.77191E-22	2.80694E-01	1.33362E-21
3.26867E-01	6.10533E-21	1.96539E-01	7.83142E-20
	a_i 54000.5 – 54500.0		cm^{-1}
9.33711E-03	1.32897E-22	3.63980E-02	1.78786E-22
1.46182E-01	3.38285E-22	3.81762E-01	8.93773E-22
2.58549E-01	4.28115E-21	1.64773E-01	4.67537E-20
	a_i 53500.5 – 54000.0		cm^{-1}
9.51799E-03	1.00252E-22	3.26320E-02	1.33766E-22
1.45962E-01	2.64831E-22	4.49823E-01	6.42879E-22
2.14207E-01	3.19594E-21	1.45616E-01	2.77182E-20
	a_i 53000.5 – 53500.0		cm^{-1}
7.87331E-03	3.38291E-23	6.91451E-02	4.77708E-23
1.29786E-01	8.30805E-23	3.05103E-01	2.36167E-22
3.35007E-01	8.59109E-22	1.49766E-01	9.63516E-21
	a_i 52500.5 – 53000.0		cm^{-1}
6.92175E-02	1.56323E-23	1.44403E-01	3.03795E-23
2.94489E-01	1.13219E-22	3.34773E-01	3.48121E-22
9.73632E-02	2.10693E-21	5.94308E-02	1.26195E-20
	a_i 52000.5 – 52500.0		cm^{-1}
1.47873E-01	8.62033E-24	3.15881E-01	3.51859E-23
4.08077E-01	1.90524E-22	8.08029E-02	9.93062E-22
3.90399E-02	6.38738E-21	8.13330E-03	9.93644E-22
	a_i 51500.5 – 52000.0		cm^{-1}
1.50269E-01	1.02621E-23	2.39823E-01	3.48120E-23
3.56408E-01	1.69494E-22	1.61277E-01	6.59294E-22
8.89713E-02	2.94571E-21	3.25063E-03	1.25548E-20
	a_i 51000.5 – 51500.0		cm^{-1}
2.55746E-01	8.49877E-24	2.94733E-01	2.06878E-23
2.86382E-01	9.30992E-23	1.21011E-01	3.66239E-22
4.21105E-02	1.75700E-21	–	–
	a_i 50500.5 – 51000.0		cm^{-1}
5.40111E-01	7.36085E-24	2.93263E-01	2.46742E-23
1.63417E-01	1.37832E-22	3.23781E-03	2.15052E-21
–	–	–	–
	a_i 50000.5 – 50500.0		cm^{-1}
8.18514E-01	7.17937E-24	1.82262E-01	4.17496E-23
–	–	–	–
–	–	–	–
	a_i 49500.5 – 50000.0		cm^{-1}
8.73680E-01	7.13444E-24	1.25583E-01	2.77819E-23
–	–	–	–
–	–	–	–
	a_i 49000.5 – 49500.0		cm^{-1}
3.32476E-04	7.00362E-24	9.89000E-01	6.99600E-24
–	–	–	–
–	–	–	–

Table 2. Coefficients for the approximation of $R_j(O_2)$

	b_i 56500.5 – 57000.0		cm^{-1}
1.07382E-21	9.95029E-21	7.19430E-21	2.48960E-20
2.53735E-20	7.54467E-20	4.48987E-20	2.79981E-19
9.72535E-20	9.29745E-19	2.30892E-20	4.08009E-17
	b_i 56000.5 – 56500.0		cm^{-1}
3.16903E-22	1.98251E-21	5.87326E-22	3.44057E-21
2.53094E-21	8.81484E-21	8.82299E-21	4.17179E-20
2.64703E-20	2.43792E-19	8.73831E-20	1.46371E-18
	b_i 55500.5 – 56000.0		cm^{-1}
1.64421E-23	9.26011E-22	2.73137E-22	1.33640E-21
9.79188E-22	2.99706E-21	3.37768E-21	1.39438E-20
1.47898E-20	1.04322E-19	4.08014E-20	6.31023E-19
	b_i 55000.5 – 55500.0		cm^{-1}
8.68729E-24	7.31056E-22	8.78313E-23	1.07173E-21
8.28170E-22	2.54986E-21	2.57643E-21	9.42698E-21
9.92377E-21	5.21402E-20	3.34301E-20	2.91785E-19
	b_i 54500.5 – 55000.0		cm^{-1}
1.20679E-24	2.44092E-22	2.64326E-23	4.03998E-22
2.53514E-22	8.53166E-22	1.29834E-21	3.74482E-21
5.12103E-21	2.65798E-20	2.10948E-20	2.35315E-19
	b_i 54000.5 – 54500.0		cm^{-1}
2.79656E-24	1.40820E-22	3.60824E-23	2.69510E-22
4.02850E-22	8.83735E-22	1.77198E-21	6.60221E-21
9.60992E-21	8.13558E-20	4.95591E-21	1.22858E-17
	b_i 53500.5 – 54000.0		cm^{-1}
2.36959E-24	1.07535E-22	2.83333E-23	2.16789E-22
3.35242E-22	6.42753E-22	1.26395E-21	5.43183E-21
4.88083E-21	5.42670E-20	3.27481E-21	1.58264E-17
	b_i 53000.5 – 53500.0		cm^{-1}
8.65018E-25	3.70310E-23	1.04351E-23	6.43574E-23
1.17431E-22	2.70904E-22	4.88705E-22	1.65505E-21
2.19776E-21	2.71172E-20	2.65257E-21	2.13945E-17
	b_i 52500.5 – 53000.0		cm^{-1}
9.63263E-25	1.54249E-23	4.78065E-24	2.97642E-23
6.40637E-23	1.46464E-22	1.82634E-22	7.12786E-22
1.64805E-21	2.37376E-17	9.33059E-22	1.13741E-20
	b_i 52000.5 – 52500.0		cm^{-1}
1.08414E-24	8.37560E-24	9.15550E-24	2.99295E-23
9.38405E-23	1.95845E-22	2.84356E-22	3.39699E-21
1.94524E-22	2.72227E-19	1.18924E-21	3.20246E-17
	b_i 51500.5 – 52000.0		cm^{-1}
1.52817E-24	1.01885E-23	1.22946E-23	4.16517E-23
9.01287E-23	2.34869E-22	1.93510E-22	1.44956E-21
1.81051E-22	5.17773E-21	9.82059E-22	6.22768E-17
	b_i 51000.5 – 51500.0		cm^{-1}
2.12813E-24	8.48035E-24	5.23338E-24	1.93052E-23
1.99464E-23	7.48997E-23	4.96642E-22	6.15691E-17
4.47504E-23	2.76004E-22	8.26788E-23	1.65278E-21
	b_i 50500.5 – 51000.0		cm^{-1}
3.81336E-24	7.32307E-24	5.60549E-24	2.04651E-23
3.36883E-22	6.15708E-17	2.09877E-23	1.07474E-22
9.13562E-24	8.41252E-22	–	–
	b_i 50000.5 – 50500.0		cm^{-1}
5.75373E-24	7.15986E-24	5.90031E-24	3.05375E-23
2.97196E-22	8.92000E-17	8.55920E-24	1.66709E-17
–	–	–	–
	b_i 49500.5 – 50000.0		cm^{-1}
6.21281E-24	7.13108E-24	3.30780E-24	2.61196E-23
1.30783E-22	9.42550E-17	2.69241E-24	1.46500E-17
–	–	–	–
	b_i 49000.5 – 49500.0		cm^{-1}
6.81118E-24	6.98767E-24	7.55667E-25	2.75124E-23
1.94044E-22	1.45019E-16	1.92236E-24	3.73223E-17
–	–	–	–

Table 3. Coefficients for the approximation of R_{jNH}(M)

	a_i 51500.5 – 52000.5		cm^{-1}
1.49005E-01	4.34218E-24	2.36517E-01	2.85712E-23
3.57333E-01	1.63079E-22	8.96800E-02	2.92845E-21
1.64118E-01	6.46829E-22	3.34613E-03	1.24288E-20
	a_i 51000.5 – 51500.0		cm^{-1}
2.34411E-01	2.22526E-24	2.77355E-01	1.19809E-23
2.72652E-01	6.65791E-23	5.37179E-02	1.49955E-21
1.61792E-01	2.60979E-22	–	–
	a_i 50500.5 – 51000.0		cm^{-1}
5.37462E-01	9.36626E-25	2.92174E-01	1.76091E-23
1.69670E-01	1.31996E-22	–	–
–	–	–	–
	a_i 50000.5 – 50500.0		cm^{-1}
7.64305E-01	3.97254E-25	2.32449E-01	2.02877E-23
–	–	–	–
–	–	–	–
	a_i 49500.5 – 50000.0		cm^{-1}
8.73785E-01	2.83903E-25	1.16752E-01	1.95469E-23
9.84455E-03	1.19731E-22	–	–
–	–	–	–
	a_i 49000.5 – 49500.0		cm^{-1}
9.78372E-01	8.85822E-26	2.19664E-02	3.97724E-23
–	–	–	–
–	–	–	–

Table 4. Coefficients for the approximation of $R_{jNH}(O_2)$

	b_i 51500.5 – 52000.0		cm^{-1}
1.10963E-24	5.45158E-24	9.20957E-24	4.03268E-23
1.16019E-22	7.12249E-22	5.98772E-23	1.79596E-22
2.85927E-22	3.49938E-21	8.86031E-22	5.84617E-17
	b_i 51000.5 – 51500.0		cm^{-1}
4.67802E-25	2.14785E-24	2.34678E-24	9.62845E-24
1.19112E-23	4.62742E-23	4.39026E-23	1.98767E-22
8.94808E-23	1.46454E-21	4.79330E-22	6.02536E-17
	b_i 50500.5 – 51000.0		cm^{-1}
4.20214E-25	8.91001E-25	2.52217E-24	9.93617E-24
1.51893E-23	6.99981E-23	3.17767E-22	5.95101E-17
1.44949E-23	3.83009E-22	–	–
	b_i 50000.5 – 50500.0		cm^{-1}
6.44408E-24	5.89743E-23	2.45136E-22	8.09304E-17
1.26908E-24	1.11346E-18	5.41633E-24	1.30923E-17
1.62561E-24	6.37674E-24	-4.14825E-24	6.40621E-22
	b_i 49500.5 – 50000.0		cm^{-1}
7.55492E-25	3.29742E-24	1.03740E-24	1.37701E-18
6.78614E-23	6.83285E-17	2.98030E-24	4.27578E-23
-1.39698E-24	6.88167E-22	-2.12512E-25	9.94586E-21
	b_i 49000.5 – 49500.0		cm^{-1}
6.45491E-25	3.28638E-23	3.40088E-23	8.17442E-17
1.83888E-25	2.79877E-24	-2.13618E-25	3.75882E-22
–	–	–	–

Table 5. Average cross sections σ_{jH} in 10^{-24} cm^2

Wave number interval (cm^{-1})	σ_{jH} (1988)	σ_{jH} (1992)
51500.5–52000.0	3.50	0.62
51000.5–51500.0	6.12	2.40
50500.5–51000.0	6.43	3.82
50000.5–50500.0	6.67	4.91
49500.5–50000.0	6.83	5.69
49000.5–49500.0	6.90	6.18

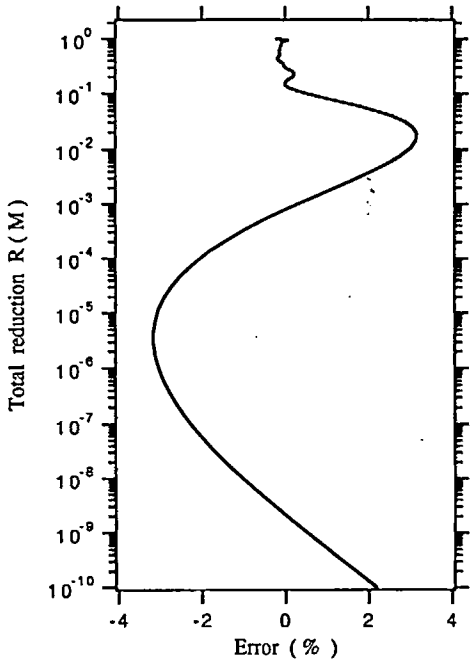

Fig. 7. Error of the total reduction factor R(M), as defined by Eq. (9)

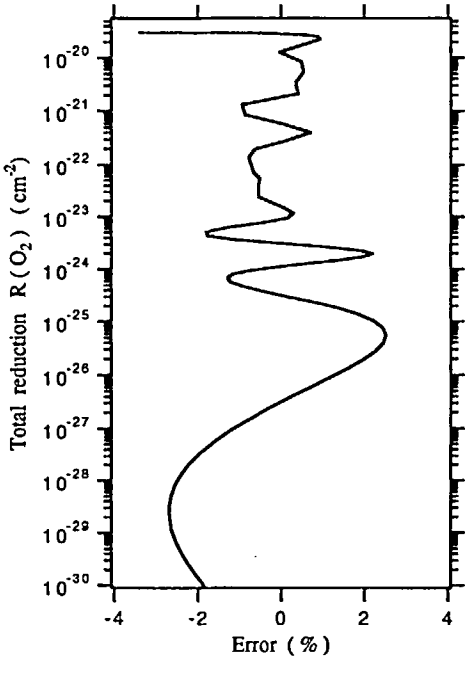

Fig. 8. Error of the total reduction factor R(O_2), as defined by an equation similar to Eq. (9)

4 Applications

The approximations developed in this paper do not depend on the value of solar irradiance in the Schumann-Runge bands.

Practical applications require, however, a knowledge of the solar irradiance in each 500 cm^{-1} wave number interval. A solar spectrum obtained on 28 February 1992 with the

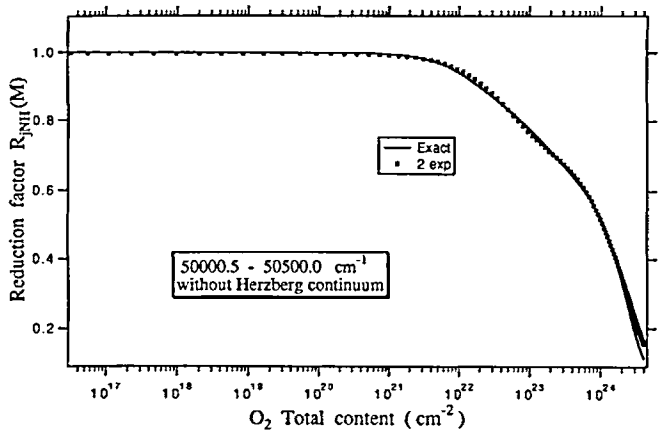

Fig. 9. Comparison between exact calculation and approximation of the reduction factor $R_{jNH}(M)$ in the 50000.5–50500.0 cm^{-1} interval when contribution of the Herzberg continuum is omitted

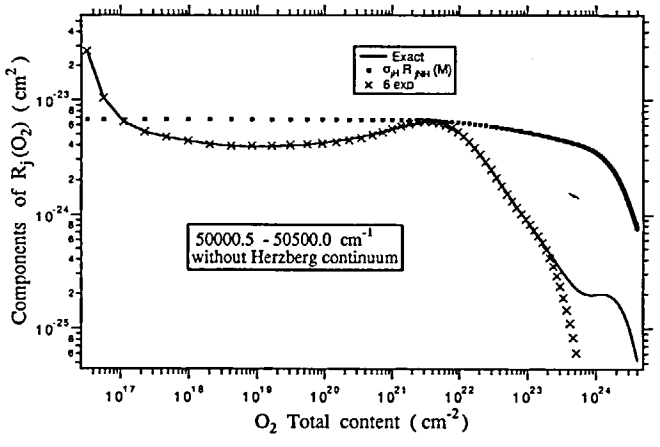

Fig. 10. Comparison between exact calculation and approximation of the reduction factor $R_{jNH}(O_2)$ in the 50000.5–50500.0 cm^{-1} interval when contribution of the Herzberg continuum is omitted. The dotted curve indicates which contribution has to be added to $R_{jNH}(O_2)$ before any computation of the O_2 photodissociation coefficient [see Eq. (12)]

SOLSTICE spectrometer on board the Upper Atmosphere Research Satellite (UARS) has been kindly provided by G. Rottman in numerical form for 1 nm resolution (London *et al.*, 1993). These data have been averaged over each of the 500 cm^{-1} intervals and the resulting irradiances are used in this section.

The first application deals with the effect of different values on the absorption by the Herzberg continuum (Yoshino *et al.*, 1988, 1992). The approximations developed in Sect. 3.2 without Herzberg continuum are suitable for such an analysis. Equations (11)–(13) indicate that an average Herzberg continuum cross section is required for each 500 cm^{-1} interval. The analytical expressions of Yoshino *et al.* (1988, 1992) have been used to compute these averaged values. The results are given in Table 5. The identification is made by the year indicated above the cross section columns.

Using data in Table 1 above 52000 cm^{-1} and in Table 3 below 52000 cm^{-1}, Eq. (11) is computed for each interval. Above 52000 cm^{-1}, the transmissions $T_j(H)$ are all equal to

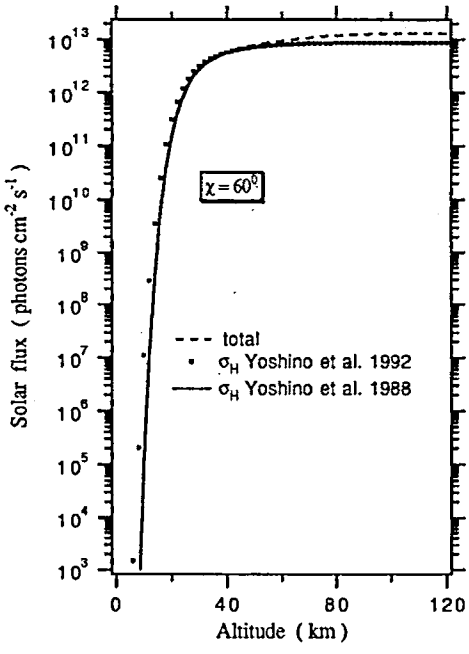

Fig. 11. Total solar flux available between 57000.0 and 49000.5 cm^{-1} as a function of height for a solar zenith angle χ of 60°. The *full* and *dotted curves* correspond respectively to the cross sections given in Table 5. The *dashed curve* represents the total flux penetrating in the Schumann-Runge bands. It merges with the full curve around 40 km

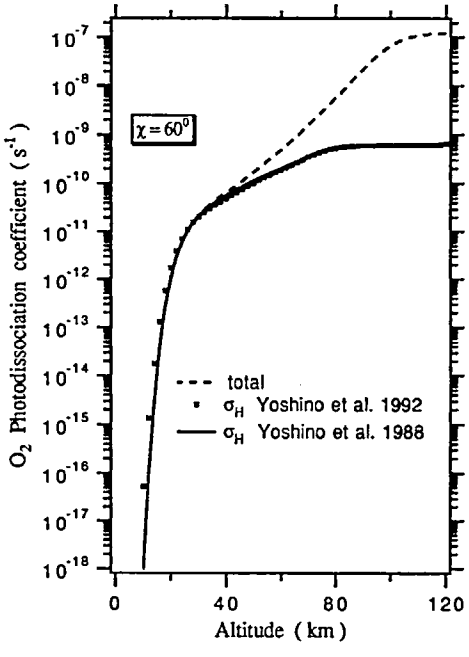

Fig. 12. O_2 photodissociation coefficient for the same conditions as those in Fig. 11

one, since the Herzberg continuum is completely negligible. The results are multiplied by the solar fluxes (London *et al.*, 1993) in each interval [Eq. (4)] and a final sum is made over the 16 intervals. Figure 11 gives the final result for the total solar radiation available in the Schumann-Runge bands as a function of altitude. A solar zenith distance χ = 60°

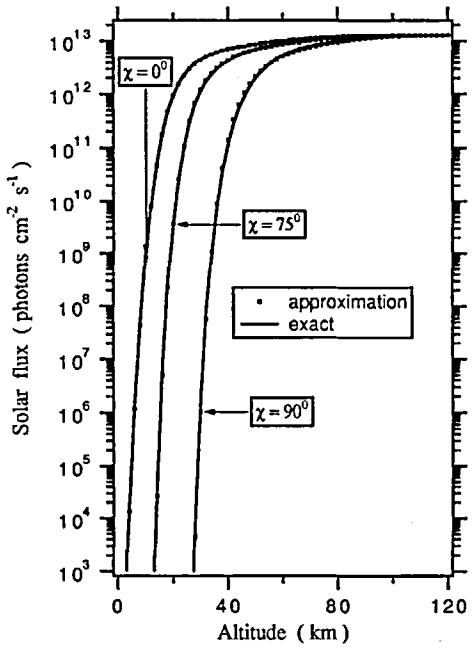

Fig. 13. Comparison between exact calculations and approximations of the total solar flux in the Schumann-Runge bands for various solar zenith angles $\chi = 0°$, 75°, and 90° as a function of altitude

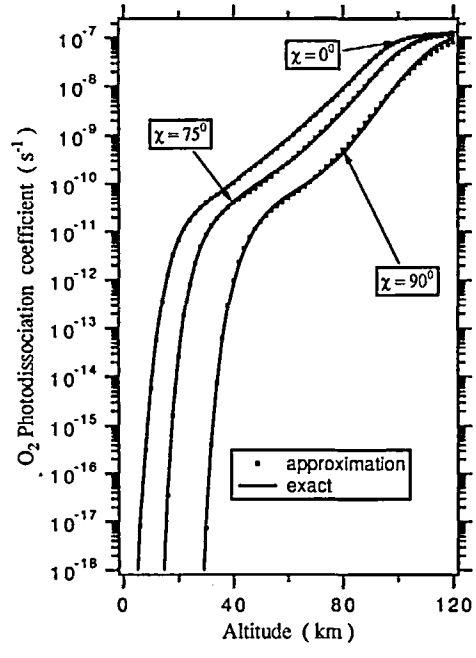

Fig. 14. Comparison between exact calculations and approximations of the O_2 photodissociation coefficient in the Schumann-Runge bands for various solar zenith angles $\chi = 0°$, 75°, and 90° as a function of altitude

has been adopted for the slant O_2 total content. Figure 11 indicates that it is possible to compute solar attenuation up to a factor of 10^{10}. The total flux is given by the dashed curve, which merges with the Herzberg continuum region around 40 km altitude. The dashed curve corresponds to the cross sections of Yoshino *et al.* (1988), but use of the 1992 values makes no difference, since the dotted and full curves are almost identical in the altitude region covered by the dashed curve. The difference resulting from the adoption of the high or low values of Table 5 becomes important in the lower stratosphere, where the total flux available is given by either the dotted or the full curve, depending on the adopted cross sections for the Herzberg continuum. It should be noted that these computations do not take into account any absorption by stratospheric and mesospheric ozone. Nevertheless, they show that precise values for the Herzberg continuum are still required below 200 nm.

A similar exercise has been done with Eq. (12) to compute the contribution of the Schumann-Runge bands to the O_2 photodissociation. The predissociation efficiency [see Eq. (2)] has been taken equal to 1 in each interval. The results are show in Fig. 12, which also extends over a range of 10^{10}. Similar conclusions as those for the total solar flux in Fig. 11 are obtained from Fig. 12.

The approximations of Sect. 3.2 are, therefore, a practical tool for analyzing the effects of various absorption cross sections in the Herzberg continuum, even in a specific wave number interval.

Allen and Frederick (1982) noted that optical paths with the same O_2 column but different zenith angles may have significantly different transmission and dissociation rates. As a consequence, they introduced a zenith angle dependent factor in the polynomial approximation of effective cross sections. Nicolet and Kennes (1989) used a similar approach. In both cases, there is a maximum value for the solar zenith angle and the approximation is a function of $\sec\chi$. It is well known that $\sec\chi$ should be replaced by a Chapman function for zenith angles greater than 65°, so that a polynomial correction depending on $\sec\chi$ should lead by itself to errors for large zenith distances.

Whereas all previous approximations cover a transmission domain down to approximately 10^{-3}, the present results have been developed down to 10^{-10}. Before attempting any polynomial correction as a function of $\sec\chi$, it is useful to investigate how exact calculations compare with the approximation when a Chapman function is used for computing the O_2 column content.

An excellent and simple approximation for the Chapman function is given by Green *et al.* (1964) for solar distances ranging from $\chi = 0°$ to 90°. If X is defined by

$$X = (a + z)/H, \tag{14}$$

where a is the Earth's radius, z the altitude, and H the atmospheric scale height, then the Chapman function $\mathrm{Ch}(\chi, X)$ is given by

$$\mathrm{Ch}(\chi, X) = \exp\left[\frac{0.5 \times \chi^2}{(1 - 0.115 \times \chi^2 - \alpha \times \chi^4)}\right], \tag{15}$$

where the solar zenith distance χ is expressed in radians. The dimensionless quantity α is given by

$$\alpha = c^{-4} - 0.115 \times c^{-2} - \left[\frac{0.5 \times c^{-2}}{\ln(c \times X)^{1/2}}\right], \tag{16}$$

with $c = \pi/2$.

Although O_2 is not exactly in perfect mixing in the model of Hedin (1991), I have nevertheless taken H as the atmospheric scale height with a mean molecular mass of 28.9 amu.

Comparisons between exact computations and approximations including Herzberg continuum (see Tables 1 and 2) are shown on Figs. 13 and 14 for three solar zenith angles 0°, 75°, and 90°. The slant O_2 total content has always been computed with Eq. (15).

The agreement between exact and approximated computations is satisfactory. The introduction of a $\sec\chi$ effect in the new approximations does not seem to provide a significant improvement. This is a consequence of the large validity domain (10^{10}), for which the new approximations have been developed.

5 Conclusions

Any exact analysis of the penetration of solar radiation in the Schumann-Runge bands of molecular oxygen between 175 nm and 205 nm requires the computation of thousands of exponentials at every grid point of a given atmospheric model. When computer resources are sufficient, it is always better to make exact computations with detailed temperature-dependent absorption cross sections. Approximations should be used only when there is a computer limitation or as a first step in the analysis of a particular problem.

The new approximation is mathematically structured as the exact calculation, i.e. a sum of exponentials. This similarity imposes the use of *non linear* least-square fitting as opposed to the *linear* techniques used in previous approximations. Instead of having 1000 terms in each 500 cm^{-1} wave number interval, only six terms are necessary to obtain a satisfactory approximation. Furthermore, in each of the 16 intervals between 49 000 and 57 000 cm^{-1}, the approximations are valid over a much larger domain (10^{10}) than has been covered in all previous approximations.

The new approximation is *robust* in the sense that no accident occurs if it is used outside of its validity domain. This results from the fact that the approximation is a sum of always-decreasing exponentials when the O_2 total content increases.

Since there is still a problem for the cross sections in the Herzberg continuum below 205 nm, two sets of approximations have been developed, one including a Herzberg continuum and the other omitting it. As a result, the potential user can make his own choice.

The approximations have been tested for various solar zenith angles and the agreement with exact computations is satifactory. The atmospheric model dependence (i.e. different vertical temperature distributions) has not been analyzed. Some work has still to be done.

Acknowledgement. I would like to thank Gary Rottman for kindly providing solar irradiance data used in this paper. Part of this work was developed during a short stay at the National Center for Atmospheric Research (NCAR), Boulder, CO. This work was supported in part by the Belgian Fonds National de la Recherche Scientifique. Topical Editor J.-C. Gérard thanks K. Minschwaner for his help in evaluating this paper.

References

Ackerman, M. and F. Biaumé, Structure of the Schumann-Runge bands from the 0-0 to the 13-0 band, *J. Molec. Spectr.*, **35**, 73–82, 1970.

Ackerman, M., F. Biaumé, and G. Kockarts, Absorption cross sections of the Schumann-Runge bands of molecular oxygen, *Planet. Space Sci.*, **18**, 1639–1651, 1970.

Allen, M. and J.E. Frederick, Effective photodissociation cross sections for molecular oxygen and nitric oxide in the Schumann-Runge bands, *J. Atmos. Sci.*, **39**, 2066–2075, 1982.

Anderson, G.P. and L.A. Hall, Stratospheric determination of O_2 cross sections and photodissociation rate coefficients: 191–215 nm, *J. Geophys. Res.*, **91**, 14 509–14 514, 1986.

Banks, P.M. and G. Kockarts, Chap. 8 in *Aeronomy, Part A*, Academic Press, New York, 1973.

Blake, A.J., An atmospheric absorption model for the Schumann-Runge bands of oxygen, *J. Geophys. Res.*, **84**, 3272–3282, 1979.

Fang, T.-M, S.C. Wofsy, and A. Dalgarno, Opacity distribution functions and absorption in Schumann-Runge bands of molecular oxygen, *Planet. Space Sci.*, **22**, 413–425, 1974.

Green, A.E.S., C.S. Lindenmeyer and M. Griggs, Molecular absorption in planetary atmospheres, *J. Geophys. Res.*, **69**, 493–504, 1964.

Hedin, A.E., Extension of the MSIS thermosphere model into the middle and lower thermosphere, *J. Geophys. Res.*, **96**, 1159–1172, 1991.

Hudson, R.D. and V.L. Carter, Predissociation in N_2 and O_2, *Canad. J. Chem.*, **47**, 1840–1844, 1969.

Johnston, H.S., M. Paige, and F. Yao, Oxygen absorption cross sections in the Herzberg continuum and between 206 and 327 K, *J. Geophys. Res.*, **89**, 11 661–11 665, 1984.

Kockarts, G., Penetration of solar radiation in the Schumann-Runge bands of molecular oxygen, in *Mesospheric models and related experiments*, Ed. G. Fiocco, pp. 160–176, D. Reidel, 1971.

Kockarts, G., Absorption and photodissociation in the Schumann-Runge bands of molecular oxygen in the terrestrial atmosphere, *Planet. Space Sci.*, **24**, 589–604, 1976.

Lewis, B.R., L. Berzins, and J.H. Carver, Decomposition of the photoabsorption continuum underlying the Schumann-Runge bands of $^{16}O_2$, I, Role of the $B^3\Sigma_u^-$ state: A new dissociation limit, *J. Quant. Spectrosc. Radiat. Transfer*, **33**, 627–643, 1985.

Lewis, B.R., L. Berzins, and J.H. Carver, Decomposition of the photoabsorption continuum underlying the Schumann-Runge bands of $^{16}O_2$, II, Role of the $1\ ^3\Pi_g$ state and collision-induced absorption, *J. Quant. Spectrosc. Radiat. Transfer*, **34**, 405–415, 1985.

London, J., G.J. Rottman, T.N. Woods and F. Wu, Time variations of solar UV irradiance as measured by the SOLSTICE (UARS) instrument, *Geophys. Res. Lett.*, **20**, 1315–1318, 1993.

Marquardt, D.W. An algorithm for least-squares estimation of nonlinear parameters, *J. Soc. Indust. Appl. Math.*, **11**, 431–441, 1963.

Minschwaner, K., G.P. Anderson, L.A. Hall, and K. Yoshino, Polynomial coefficients for calculating O_2 Schumann-Runge cross sections at 0.5 cm^{-1} resolution, *J. Geophys. Res.*, **97**, 10 103–10 108, 1992.

Minschwaner, K., R.J. Salawitch, and M.B. McElroy, Absorption of solar radiation by O_2: implications for O_3 and lifetimes of N_2O, $CFCl_3$, and CF_2Cl_2, *J. Geophys. Res.*, **98**, 10 543–10 561, 1993.

Minschwaner, K. and D.E. Siskind, A new calculation of nitric oxide photolysis in the stratosphere, mesosphere, and lower thermosphere, *J. Geophys. Res.*, **98**, 20 401–20 412, 1993.

Murtagh, D.P., The O_2 Schumann-Runge system: new calculations of photodissociation cross-sections, *Planet. Space Sci.*, **36**, 819–828, 1988.

Murtagh, D.P., New calculations of photodissociation cross-sections in the O_2 Schumann-Runge system, *Proc. Ninth ESA/PAC Symposium on European rocket and balloon programmes*, 49–53, 1989.

Nicolet, M. and W. Peetermans, Atmospheric absorption in the O_2 Schumann-Runge band spectral range and photodissociation rates in the stratosphere and mesosphere, *Planet. Space Sci.*, **28**, 85–103, 1980.

Nicolet, M. and R. Kennes, Aeronomic problems of molecular oxygen photodissociation – VI. Photodissociation frequency and transmittance in the spectral range of the Schumann-Runge bands, *Planet. Space Sci.*, **37**, 459–491, 1989.

Press, W. H., B. P. Flannery, S. A. Teukolsky, and W. T. Vetterling, *Numerical recipes in Pascal,* Cambridge University Press, 1989.

Toumi, R. and S. Bekki, Sensitivity of stratospheric composition to oxygen absorption of solar radiation (175–210 nm), *J. Atmos. Chem,* **18,** 57–73, 1994.

U.S. Standard atmosphere, 1976, U.S. Government Printing Office, Washington D.C., 1976.

W.M.O. (Ed.) *Atmospheric Ozone 1985, Assessment of our understanding of the processes controlling its present distribution and change,* Vol. 1, pp. 349–392, 1986.

Yoshino,K., D. E. Freeman, J. R. Esmond, and W. H. Parkinson, High-resolution absorption cross section measurements and band oscillator strengths of the (1,0)–(12,0) Schumann-Runge bands of O_2, *Planet. Space Sci.,* **31,** 339–353, 1983.

Yoshino, K., D. E. Freeman, and W. H. Parkinson, Atlas of the Schumann-Runge absorption bands of O_2 in the wavelength region 175–205 nm, *J. Phys. Chem. Ref. Data,* **13,** 207–227, 1984.

Yoshino,K., D. E. Freeman, J. R. Esmond, and W. H. Parkinson, High-resolution absorption cross sections and band oscillator strengths of the Schumann-Runge bands of oxygen at 79 K, *Planet. Space Sci.,* **35,** 1067–1075, 1987.

Yoshino, K., A. S.-C. Cheung, J. R. Esmond, W. H. Parkinson D. E. Freeman, S. L. Guberman, A. Jenouvrier, B. Coquart, and M. F. Merienne, Improved absorption cross-sections of oxygen in the wavelength region 205–240 nm of the Herzberg continuum, *Planet. Space Sci.,* **36,** 1469–1475, 1988.

Yoshino, K., J. R. Esmond, A. S.-C. Cheung, D. E. Freeman, and W. H. Parkinson, High-resolution absorption cross section in the transmission window region of the Schumann-Runge bands and the Herzberg continuum of O_2, *Planet. Space Sci.,* **40,** 185–192, 1992.

This article was processed by the aukthor using Springer-Verlag Plain-TEX ann geo macro package 1.0 and the AMS fonts, developed by the American Mathematical Society.